Fast fatigue characterization by infrared thermography for additive manufacturing

Corentin Douellou, Xavier Balandraud, Emmanuel Duc, Benoit Verquin, Fabien Lefebvre, Frédéric Sar

Available online at www.sciencedirect.com

ScienceDirect

Structural Integrity Procedia 00 (2019) 000–000

Structural Integrity Procedia

www.elsevier.com/locate/procedia

Fatigue Design 2019

Fast fatigue characterization by infrared thermography for additive manufacturing

Corentin Douellou[a]*, Xavier Balandraud[a], Emmanuel Duc[a], Benoit Verquin[b], Fabien Lefebvre[b], Frédéric Sar[c]

[a]*Université Clermont Auvergne, CNRS, SIGMA Clermont, Institut Pascal, F-63000 Clermont–Ferrand, France*
[b]*Cetim, 60304 Senlis, France*
[c]*AddUp, 63118 Cébazat, France*

Abstract

High cooling rates and strong temperature gradients occurring during additive manufacturing (AM) by laser beam melting (LBM) are known to affect mechanical performances of the produced parts, and particularly fatigue properties. Mechanical properties strongly depend on the process parameters such as laser power, scan speed and laser spot size. A fatigue analysis was performed in this study by using infrared thermography to assess heat sources associated with fatigue damage. In particular, mechanical dissipation was identified thanks to suitable acquisition parameters. A model for the relationship between mechanical dissipation and mechanical solicitation was proposed and applied to two promising steels in LBM AM field, namely maraging 18Ni300 and L40 tool steel.

Peer-review under responsibility of the Fatigue Design 2019 Organizers.

Keywords: Additive Manufacturing; Fatigue; Infrared thermography; Laser Beam Melting; Mechanical dissipation; Self-heating

* Corresponding author. Tel.: +33 6 04 13 98 53
E-mail address: corentin.douellou@sigma-clermont.fr

Peer-review under responsibility of the Fatigue Design 2019 Organizers.

1. Introduction

The term "additive manufacturing" (AM) refers to a large group of technologies that allow the production of a part through a layer-by-layer addition of matter. The present study focuses on metal parts manufactured by laser beam melting (LBM) of metal powder beds. The achievable mechanical properties for a given material strongly depend on the manufacturing conditions, parameters and strategy. The multi-scale and multi-physical nature of LBM process makes it very difficult to fully understand how to obtain properties that are both good and reproducible. In general, the microstructure – particularly influenced by high cooling rates and thermal gradients – is fine and oriented in the laser path direction [1, 2], which leads to materials harder than the standards, with good yield strength but low ductility [2-6]. Fatigue performances of LBM AM metals are generally lower than that obtained by conventional manufacturing means. It is also well recognized that the size and quantity of porosities formed during the production of a part have a major influence on the mechanical quality of the part, particularly on fatigue performance because porosities are crack initiators. Porosities are also known as responsible for large dispersion on fatigue test results [1, 6-9].

Conventional fatigue tests for the determination of S-N (Stress-Number of cycles) curves are time-consuming and expensive. Determining a full S-N curve usually requires several tens of samples, especially to identify the fatigue limit. The cost of such a number of LBM AM samples being of several thousands of euros as an order of magnitude, alternative solutions need to be found. It is known since the beginning of the 20th century with the works of Stromeyer [10] that cyclic loading is accompanied by material self-heating. However, because of the lack of advanced technologies, this phenomenon has not been extensively studied before the 80s (see the works of Luong *et al.* [11, 12] and La Rosa *et al.* [13]). Under mechanical loading, temperature variations of a material sample are due to thermoelastic couplings and mechanical irreversibility such as viscosity, plasticity, cracks or fatigue damage depending on the material and the loading mode. Heat exchanges by conduction, contact, convection and radiation are also involved in the thermal response of the material. Chrysochoos *et al.* [14] proposed to reconstruct the heat source (in W/m^3) due to changes in the material mechanical state from temperature maps obtained by infrared (IR) thermography. The heat diffusion equation is employed for that purpose, with some hypotheses due to the fact that IR thermography only provides surface temperatures. Studying heat sources instead of temperatures enables to extract the calorific signature of mechanical mechanisms from the global thermal response of the sample. In particular, in the case of fatigue characterization, the focus is on the part of the heat source due to irreversible damage, named mechanical dissipation or intrinsic dissipation [15-17].

The present paper is organized as follows. Section 2 describes the experimental procedure and the analysis of results obtained on two different steels: maraging steel and L40 tool steel. The former is often used in AM because of its good mechanical properties and good weldability. The latter is a quite recent and promising alloy for AM because of possible applications to rapid and tailored tooling (injection mold with conformal cooling for example). Section 3 presents an original approach of mathematical modeling of the mechanical dissipation behavior as a function of the stress level. Analysis and discussion are presented in Section 4.

2. Experimental procedure and analysis

2.1 Experimental setup and methodology

The objective of the experimental procedure was to identify the mechanical dissipation (in W/m^3) due to fatigue damage. Let us recall that mechanical dissipation is the part of the heat source due to irreversible mechanical phenomena. By *heat source*, we mean the heat power density accompanying changes in the material mechanical state. Whereas heat sources can be positive (heat release) or negative (heat absorption), mechanical dissipation is always positive. Fig. 1 presents the experimental approach. Several points can be detailed:

- samples were flat, 1 mm thick. Note that plane measurement surfaces are simpler to manage than cylindrical ones in terms of thermal emissivity. Note also that thin sheet enables us to consider surface temperatures as representative of the thermal state in the thickness;
- two “references” in contact with the upper and lower jaws of the testing machine allowed us to track the temperature variations of the environment (in particular by conduction with the jaws) [18]. Disturbances can then be removed from the temperature measured in the gauge zone of the sample subjected to mechanical

loading. In practice, temperature change of the gauge zone was defined as the difference between its average temperature and the mean temperature of the two references;

- surfaces observed by the IR camera were painted matt black to increase thermal emissivity (0.95) and the surrounding was covered by blackout curtains to avoid disturbances in the IR range;
- various sine loadings in tension was applied for 5 min at a frequency of 30 Hz (9000 cycles in total) with a load ratio of 0.1 in order to avoid buckling, using a 15 kN MTS testing machine;
- temperature fields were captured by a Cedip Jade III camera at 100 Hz and averaged in real time over an integer number of cycles (here 30) in order to capture the effect of mechanical dissipation only. Indeed, heat release and absorption due to thermoelastic couplings cancels out over a thermodynamical cycle.

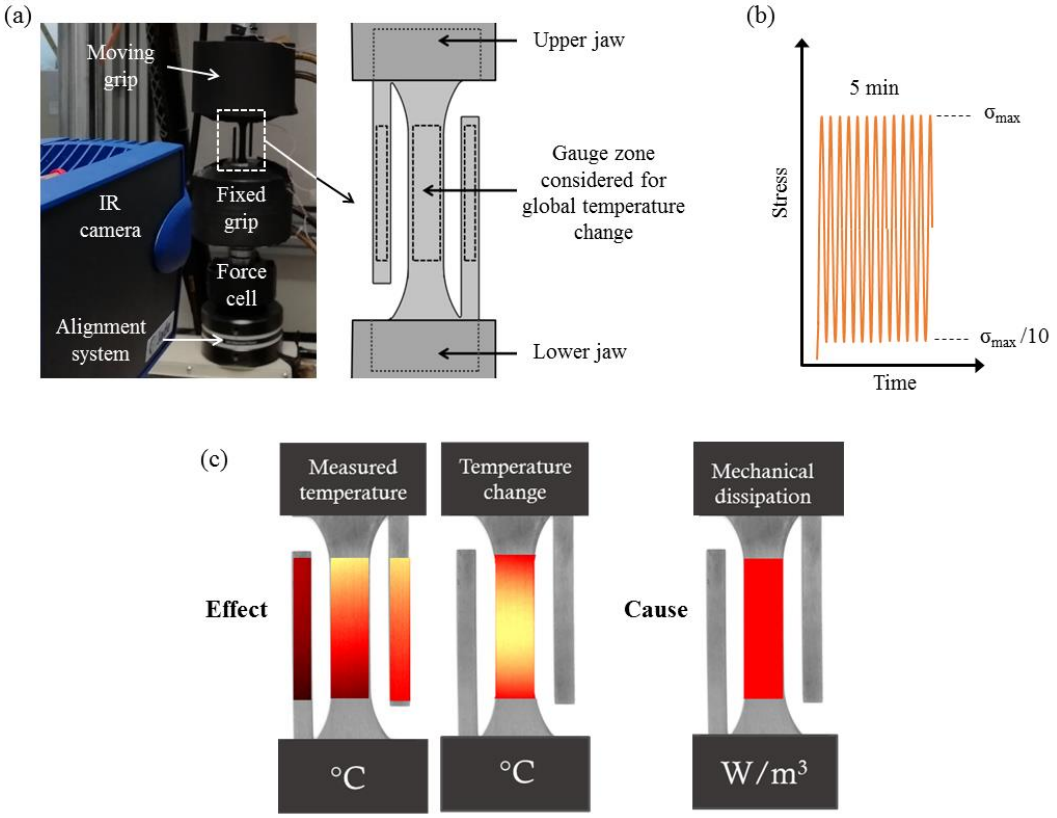

Fig. 1. Experimental approach; (a) photograph of the experiment with a detailed view of the sample geometry; (b) mechanical loading; (c) illustration of the data processing to identify mechanical dissipation.

Thermal signal processing consisted in using the mean temperature change of the gauge zone and a zero-dimensional (0D) version of the heat diffusion equation to calculate the mechanical dissipation [18]:

$$d_1(t) = \rho C \left(\frac{\mathrm{d}\theta(t)}{\mathrm{d}t} + \frac{\theta(t)}{\tau_{0D}} \right) \quad (1)$$

where d_1 is the mechanical dissipation and θ the mean temperature change averaged over an integer number of cycles. Such a time averaging operation removes the temperature oscillation associated with thermoelastic coupling. Material parameters are the density ρ and the specific heat C. Parameter τ_{0D} is a time constant characterizing the ability of the gauze zone to exchange heat with its surrounding, to be preliminary identified from a natural return to thermal equilibrium after homogeneous heating. Note that mechanical dissipation can be considered as homogeneous over the

gauge section because of the homogeneity of the stress field. Homogeneity of the heat source field justifies the use of the 0D approach, see [18] for more details.

The complete loading procedure for fatigue characterization consisted in loading the sample by blocks of increasing amplitude, until sample failure. Fig. 2 (a) shows an illustration of the mechanical loading. The 5-minute duration of each block is short enough so that the sample is not too damaged when it enters the High Cycle Fatigue range, but long enough to reach a steady thermal regime (θ constant). Indeed, the order of magnitude of τ_{0D} was estimated to 1 min for the type of materials considered in the present study (steels) and our sample's environment. A duration of at least $4\tau_{0D}$ must be respected to reach steady thermal regime. Waiting periods of 5 min were imposed between two successive loading blocks. Fig. 2 (b) shows an example of thermal response obtained for a 18Ni300 maraging sample, and Fig. 2 (c) shows the mechanical dissipation as a function of time deduced from this thermal response. It can be seen that mechanical dissipation is nearly constant over a loading block, although the value slightly decreases along the last blocks.

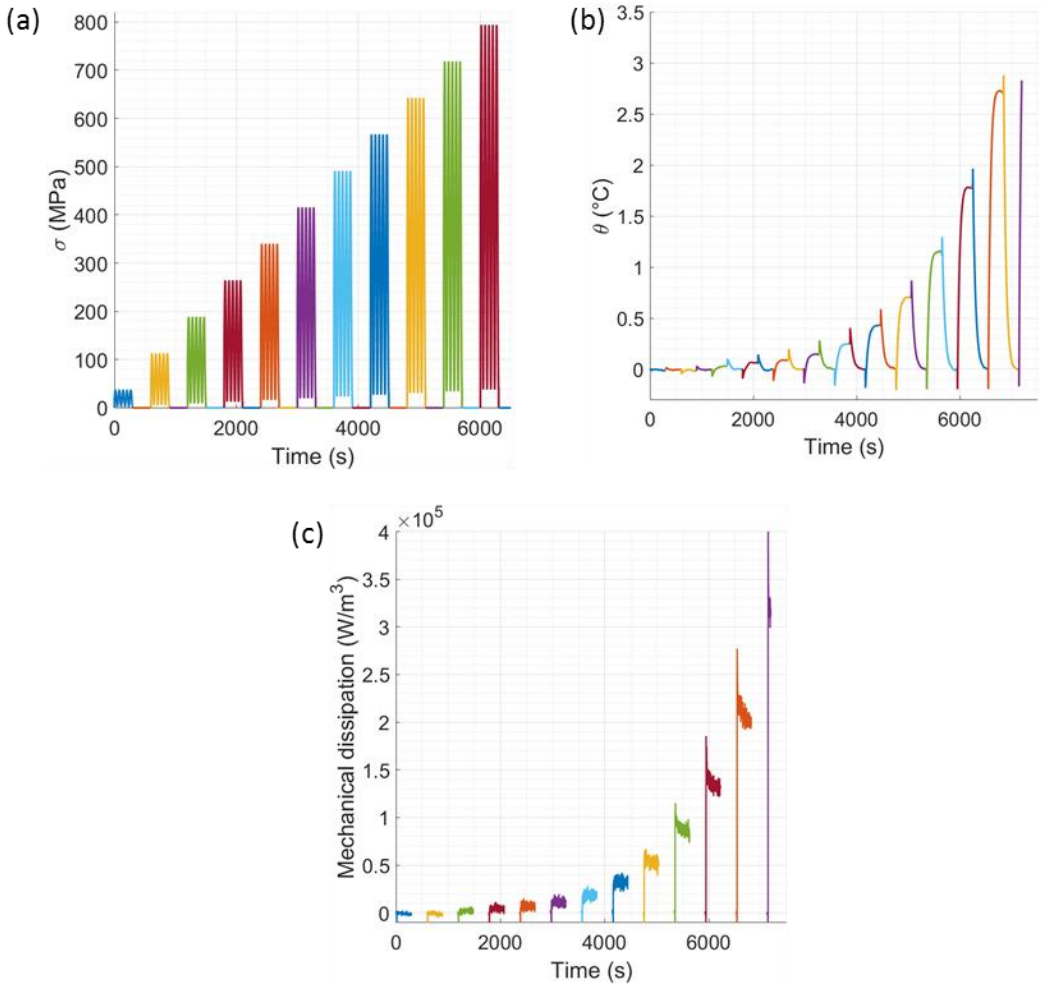

Fig. 2. Example of result for a maraging 18Ni300 sample; (a) schematic view of the mechanical loading applied; (b) thermal response; (c) mechanical dissipation as a function of time during cyclic loading blocks deduced from the thermal response.

Fig. 3 shows the averaged mechanical dissipation as a function of the maximum stress for each loading block. Luong proposed a method for estimating the fatigue limit [12]: the latter is defined as the stress value at the intersection

of two tangents (curve start and end tangents), leading here to a fatigue limit of 621 MPa. The method aims to estimate the transition point between two regimes in the mechanical dissipation behavior (respectively under and above the fatigue limit).

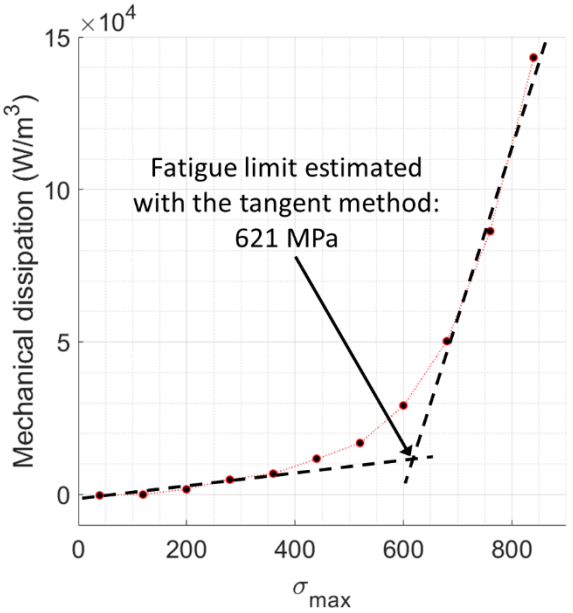

Fig. 3. Mechanical dissipation as a function of the maximum stress of the loading block for a maraging 18Ni300 sample, and illustration of the graphical criterion for estimating the fatigue limit (two-tangent method proposed by Luong [12]).

2.2 Results on two different materials

The experimental procedure was applied to two different materials: 18Ni300 maraging steel and L40 tool steel, both manufactured by LBM AM by the AddUp company, Cébazat, France. Tensile strengths and Rockwell's hardnesses are given in Table 1. Note that these value are given for as-built materials in the *x* or *y* direction (perpendicular to the manufacturing direction *z*). The process parameters are not specified here because of confidentiality concerns, and because they do not have a major influence in the scope of the study. It can be simply indicated that the parameter sets were optimized to maximize material density. Samples were first prepared in the form of plates. Surfaces were then resurfaced by grinding. Finally, they are cut to the desired geometry by water jet cutting (see Fig. 1 (a) for the geometry). Table 1 provides the material properties to be used in equation (1) for mechanical dissipation calculation. Densities and specific heat capacities were taken from the literature, while τ_{0D} was measured from natural return to thermal equilibrium.

Table 1. Material properties and parameters for 0D mechanical dissipation calculation (material properties from [19, 20]).

	18Ni300 maraging	L40 tool steel
Ultimate tensile strength (MPa)	1150	1500
Rockwell's hardness (HRC)	45	48
Density (kg.m^{-3})	8100	7780
Specific heat (J.kg^{-1}.K^{-1})	440	442
τ_{0D} (s)	48	45

Three samples of both materials coming from the same manufacturing batch were tested. The six experimental datasets of mechanical dissipation *vs* maximal stress are presented in Fig. 4. Following comments can be done from this graph:

- at a given stress level, mechanical dissipation in maraging is much higher than in the L40;
- samples made in the same material did not all break in the same loading block. Some of them may have failed sooner because of localized defects such as a big porosity at the sample surface. Even though, it can be noted that for each of the two materials, the three samples give relatively close values of mechanical dissipation for a given loading level. The mechanical dissipation value may then be considered as a pretty reliable quantity not affected by the biggest porosities at the surface.

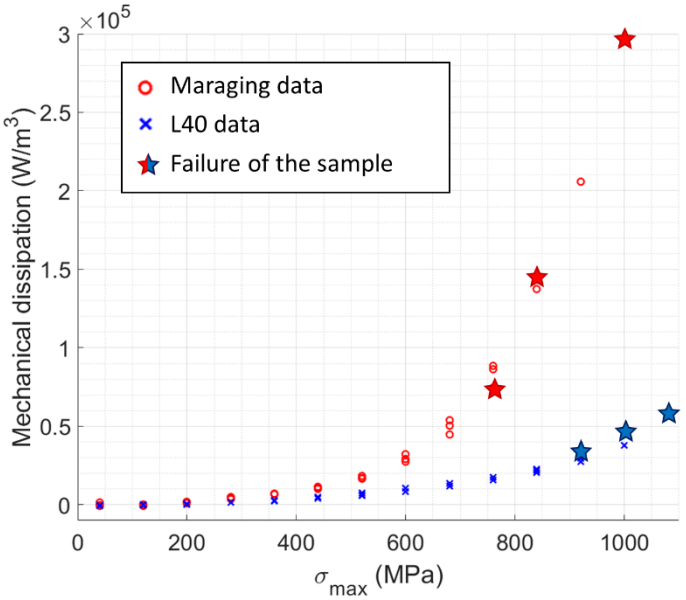

Fig. 4. Experimental results obtained for the two materials (red circles for maraging data and blue crosses for L40 data). Each material was tested three times using three samples from the same manufacturing batch.

Table 2 shows the fatigue limit estimated *via* the two-tangent method. The two materials clearly exhibit a difference in terms of fatigue limit using this method: the average fatigue limits are equal to 619 MPa and 725 MPa for maraging steel and L40 tool steel respectively. It has also been raised in previous work [17] that the method may be used to compare the performances of different manufacturing strategies.

Table 2. Fatigue limits estimated with the Luong's two-tangent method.

	18 Ni300 maraging	L40 tool steel
Sample 1	651 MPa	763 MPa
Sample 2	622 MPa	741 MPa
Sample 3	585 MPa	671 MPa

However, one would need more information about the reliability of the method for industrial applications, or for comparing materials with close behaviors. Indeed, although the dispersions on the calculated mechanical dissipation are low, the results on the fatigue limit that are provided by the Luong's two-tangent method [12] are quite dispersed (nearly 100 MPa difference over the three samples). This raises the question of the relevance of the criterion in terms of its precision and robustness. The model proposed in the following section opens prospects to another definition of the transition between the two regimes.

3. Mathematical modeling of the mechanical dissipation behavior

Several works [21-24] pointed that the evolution of the mechanical dissipation with the stress amplitude follows two regimes: a primary regime at low loading level (under the fatigue limit) and a secondary regime at high loading level (above the fatigue limit). The primary regime has been shown in the latter works to have a slight quadratic tendency: the amount of dissipated energy per cycle depends on the square of the loading amplitude. Concerning the secondary regime, the behavior strongly depends on the material and no general tendency has been raised. In the present work on steels manufactured by LBM, the end of experimental data (*i.e.* in the secondary regime) appears to be well described by an exponential curve. The transition between the two regimes, theoretically corresponding to the fatigue limit, is not clear though. So a model is proposed in equation (2) as follows:

$$d_1 = f_1(\sigma_{max}) + f_2(\sigma_{max}) \tag{2}$$

with

$$f_1(\sigma_{max}) = a \times {\sigma_{max}}^2 \times \frac{1}{\pi}\left[arctan\left(\frac{\sigma_{max} - \sigma_{trans}}{k}\right) + \frac{\pi}{2}\right] \tag{3}$$

$$f_2(\sigma_{max}) = b \times e^{c \times \sigma_{max}} \times \frac{1}{\pi}\left[arctan\left(\frac{\sigma_{trans} - \sigma_{max}}{k}\right) + \frac{\pi}{2}\right] \tag{4}$$

This expression comprises a quadratic part and an exponential part illustrated in Fig. 5 (a) by the blue and red curves respectively. Both parts are weighted by arctan functions, illustrated in Fig. 5 (b), to make a continuous junction between the primary and secondary regimes. The model is governed by five parameters:

- *a* is the shape factor of the primary regime;
- *b* and *c* are the shape factors of the secondary regime;
- σ_{trans} defines the position of the transition zone (see Fig. 5 (b)), and *k* defines its spreading. The larger k is, the smoother the transition will be.

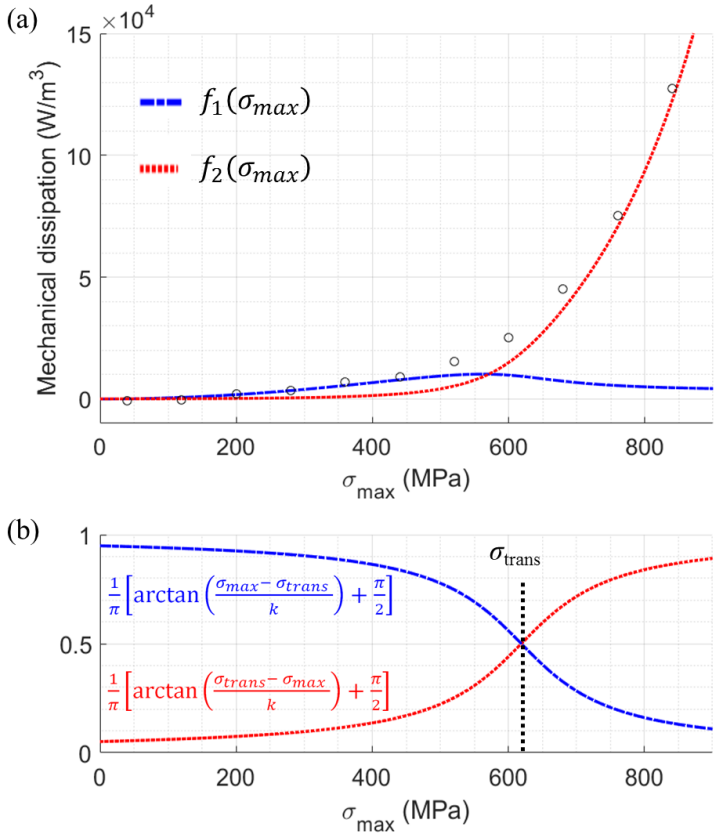

Fig. 5. Illustration of the model considered for the mechanical dissipation behavior; (a) two main parts of the expression; (b) arctan functions used to weight the two parts of the expression.

4. Analysis and discussion

The model proposed in Section 3 was used to fit the data obtained with three maraging samples and three L40 samples: see Figs. 6 (a) and (b) respectively. Table 3 summarizes the model parameters obtained after fitting. The objective here is twofold:

- validating the versatility of the model, i.e. its ability to adjust to both L40 and maraging data,
- validating its ability to follow the slight differences between samples of the same material (inter-sample dispersion). As the 0D method used for mechanical dissipation calculation is based on a spatial averaging, the latter dispersion is assumed not to be strongly influenced by the local defects that cause sample failures. The inter-sample dispersion may then be explained by complex mechanisms occurring during the manufacturing process, leading to different thermal histories and microstructures.

For this purpose, only shape parameters *a*, *b*, *c* and *d* were left free for optimization, whereas σ_{trans} and *k* were fixed. The σ_{trans} value was set to the average fatigue limit value obtained by the two-tangent method (see Table 2). After preliminary tests, parameter *k* was set at 100 MPa to allow a smooth transition between the two regimes and give flexibility to the model.

Figs. 6 (c) and (d) show the residuals between the experimental data and the fitted curves for maraging and L40 respectively. A few points at very high stress level show relatively high residuals (up to 11 kW.m^{-3}). This result is not yet well understood but may be due to a lack of robustness in the optimization algorithm. Apart from these points, residuals stay below 1 kW.m^{-3}. This result is particularly interesting as it stays in the order of magnitude of the experimental uncertainties. This result validates the ability of the model to adjust to L40 and maraging data. It also

validates its ability to follow slight differences between samples of the same material, opening perspectives for a statistical analysis about dispersion on the mechanical dissipation behavior between several samples of the same strategy, and for the construction of a more reliable criterion for fatigue limit estimation.

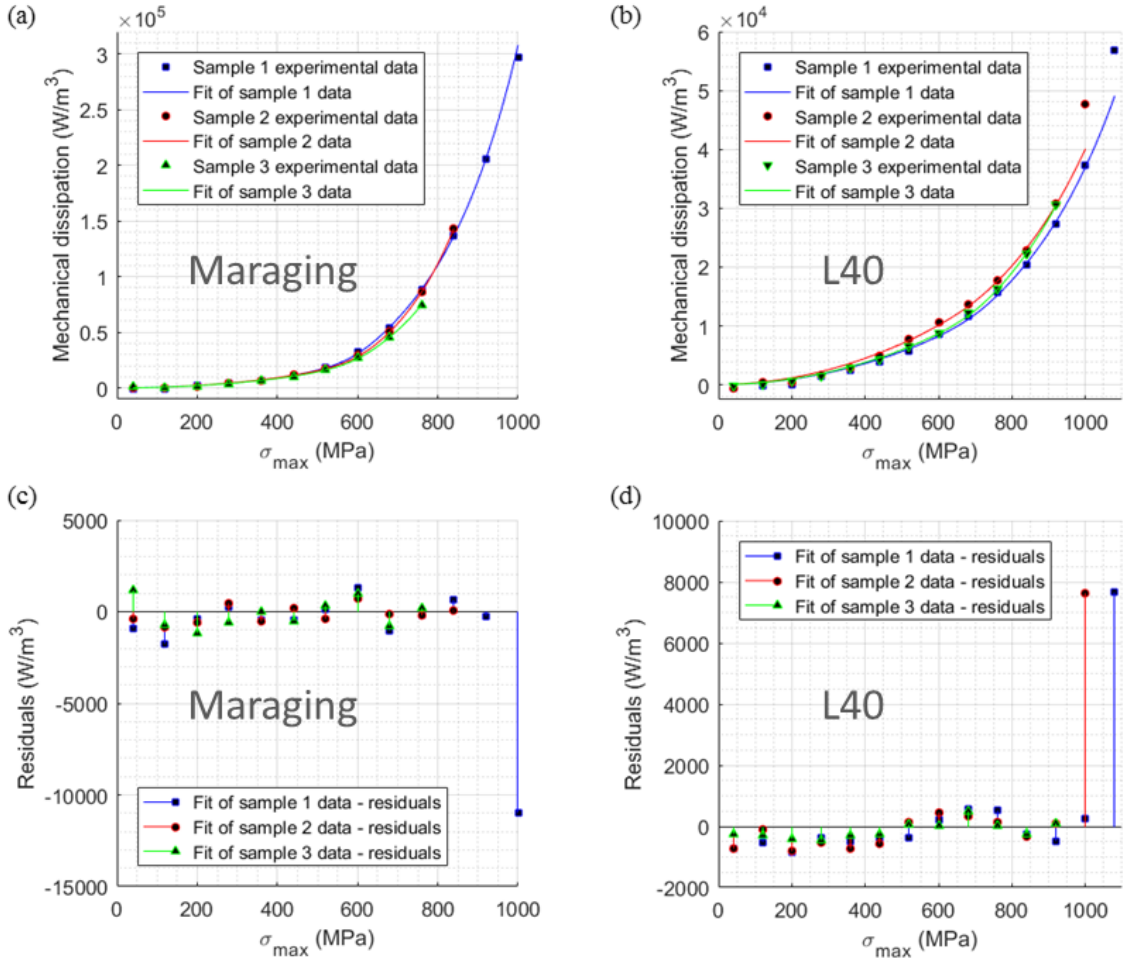

Fig. 6. Application of the model to experimental data; (a) fitting of the three maraging curves; (b) residuals between fitted curves and experimental data for maraging; (c) fitting of the three L40 curves; (d) residuals between fitted curves and experimental data for L40.

Table 3. Model parameters for each sample tested.

	Sample	a (W.m^{-3}.MPa^{-1})	b (W.m^{-3})	c (MPa^{-1})	k (MPa)	σ_{trans} (MPa)
Maraging	1	0.049	2618	0.0048	100	619
	2	0.055	1157	0.0058	100	619
	3	0.049	1725	0.0051	100	619
L40	1	0.022	1190	0.0034	100	725
	2	0.027	1465	0.0033	100	725
	3	0.023	1101	0.0036	100	725

5. Conclusion

The present study relied on an experimental approach by infrared thermography for fast fatigue characterization. Heat source reconstruction was performed in the framework of a so-called 0D approach, with specific thermal acquisition parameters to measure mechanical dissipation associated to fatigue damage only. The procedure was applied to two steels manufactured by laser beam melting: three maraging samples and three L40 samples were tested. The results reveal reproducible mechanical dissipation values despite the fact that that fatigue performance is in general highly dispersed due to the biggest surface porosities. A model was proposed for the mechanical dissipation behavior as a function of the stress level. It is based on the smooth transition between two regimes when loading level increases. Application to experimental data demonstrated the ability of the model to fit into the different experimental data sets. The ability of the model to follow slight differences between samples of the same material was also demonstrated, opening perspectives for a statistical analysis. Finally, it can be noted that comparison with conventionally manufactured materials (rolled, HIPed, machined) would be possible with the same method and highly valuable for further analysis.

Acknowledgements

The authors gratefully acknowledge the Région Auvergne Rhône Alpes (Ressourcement en fabrication additive) for their financial aid, and the company AddUp, Cébazat, France, for their support during this research. Authors would also like to thank Dr. Cécile Mattrand, Sigma Clermont Engineering School for the discussion about the model and its potential use for statistical analysis.

References

[1] Riemer, A., Leuders, S., Thöne, M., Richard, H. A., Tröster, T., Niendorf, T., 2014. On the fatigue crack growth behavior in 316L stainless steel manufactured by selective laser melting. Engineering Fracture Mechanics 120, 15–25.
[2] Röttger, A., Geenen, K., Windmann, M., Binner, F., Theisen, W., 2016. Comparison of microstructure and mechanical properties of 316 L austenitic steel processed by selective laser melting with hot-isostatic pressed and cast material. Materials Science and Engineering A 678, 365–376.
[3] Hermann Becker, T., Dimitrov, D., 2016. The achievable mechanical properties of SLM produced Maraging Steel 300 components. Rapid Prototyping Journal 22(3), 487–494.
[4] Edwards, P., Ramulu, M., 2014. Fatigue performance evaluation of selective laser melted Ti-6Al-4V. Materials Science and Engineering A 598, 327–337.
[5] Cain, V., Thijs, L., Van Humbeeck, J., Van Hooreweder, B., Knutsen, R., 2015. Crack propagation and fracture toughness of Ti6Al4V alloy produced by selective laser melting. Additive Manufacturing 5, 68–76.
[6] Rafi, H. K., Starr, T. L., Stucker, B. E., 2013. A comparison of the tensile, fatigue, and fracture behavior of Ti-6Al-4V and 15-5 PH stainless steel parts made by selective laser melting. International Journal of Advanced Manufacturing Technology 69(5–8), 1299–1309.
[7] Santos, L. M. S., Ferreira, J. A. M., Jesus, J. S., Costa, J. M., Capela, C., 2016. Fatigue behaviour of selective laser melting steel components. Theoretical and Applied Fracture Mechanics 85, 9–15.
[8] Read, N., Wang, W., Essa, K., Attallah, M. M., 2015. Selective laser melting of AlSi10Mg alloy: Process optimisation and mechanical properties development. Materials and Design 65, 417–424.
[9] Yadollahi, A., Shamsaei, N., 2017. Additive manufacturing of fatigue resistant materials: Challenges and opportunities. International Journal of Fatigue 98, 14–31.
[10] Stromeyer, C. E., Dalby, W. E., 1914. The determination of fatigue limits under alternating stress conditions, Proc. R. Soc. Lond. A, 90, 620, 411–425.
[11] Dang Van, K., Luong, M.P., 1993. Method and apparatus for determining the fatigue limit of a material. patent FR2692988 (A1).
[12] Luong M.P., 1998. Fatigue limit evaluation of metals using an infrared thermographic technique. Mechanics of Materials 28, 155–163.
[13] La Rosa G., Risitano A., 2000. Thermographic methodology for rapid determination of the fatigue limit of materials and mechanical components. International Journal of Fatigue 22, 65–73.
[14] Chrysochoos, A., Peyroux, R., 1998. Experimental analysis and numerical simulation of thermomechanical couplings in solid materials. Revue Générale de Thermique 37, 582–606.
[15] Boulanger, T., Chrysochoos, A., Mabru, C., Galtier, A., 2004. Calorimetric analysis of dissipative and thermoelastic effects associated with the fatigue behavior of steels. International Journal of Fatigue 26, 221–229.
[16] Delpueyo, D., Balandraud, X., Grédiac, M., Stanciu, S., Cimpoesu, N., 2018. A specific device for enhanced measurement of mechanical dissipation in specimens subjected to long-term tensile tests in fatigue. Strain 54, e12252.

[17] Douellou, C., Balandraud, X., Duc, E., 2019. Fatigue Characterization of 3D-Printed Maraging Steel by Infrared Thermography. In: Kramer, S., Jordan, J., Jin, H., Carroll, J., Beese, A. (eds) Mechanics of Additive and Advanced Manufacturing, Volume 8, pp 5-9. Conference Proceedings of the Society for Experimental Mechanics Series. Springer, Cham.
[18] Jongchansitto, P., Douellou, C., Preechawuttipong, I., Balandraud, X., 2019. Comparison between 0D and 1D approaches for mechanical dissipation measurement during fatigue tests. Strain 55(3), e12307.
[19] MatWeb: EOS MS1 Maraging Steel for DMLS 3D Printing. Available at http://www.matweb.com/search/DataSheet.aspx?MatGUID=e9f7cb19eb81450d8f67966151bd1802
[20] NanoSteel: BLDRmetalTM L-40 (2018). Available at https://nanosteelco.com/images/uploads/resources/L40_Data_Sheet_June_2018_web.pdf
[21] Mareau, C., Favier, V., Weber, B., Galtier, A., Berveiller, M., 2012. Micromechanical modeling of the interactions between the microstructure and the dissipative deformation mechanisms in steels under cyclic loading. International Journal of Plasticity 32–33, 106-120.
[22] Doudard, C., Calloch, S., Hild, F., Cugy, P., Galtier, A., 2004. Identification of the scatter in high cycle fatigue from temperature measurements. Comptes rendus mécanique 332, 795–801.
[23] Munier, R., Doudard, C., Calloch, S., Weber, B., 2014. Determination of high cycle fatigue properties of a wide range of steel sheet grades from self-heating measurements. International Journal of Fatigue 63, 46–61.
[24] Munier, R., Doudard, C., Calloch, S., Weber, B., 2017. Identification of the micro-plasticity mechanisms at the origin of self-heating under cyclic loading with low stress amplitude. International Journal of Fatigue 103, 122–135.